Progress In Electromagnetics Research B, Vol. 11, 223–243, 2009

EFFICIENT TRANSMISSION LINE MODELING SENSITIVITY ANALYSIS EXPLOITING RUBBER CELLS

P. A. W. Basl †, M. H. Bakr, and N. K. Nikolova

McMaster University
Hamilton, ON, Canada

Abstract—The adjoint variable method is applied for the first time to perform sensitivity analysis with transmission line modeling exploiting rubber cells. Rubber cells allow for the conformal modeling of off-grid boundaries in the transmission line modeling computational domain using modified tensor properties. The scattering matrix of the rubber cell is analytically dependent on the dimensions of the modeled discontinuities. Using this property, an exact adjoint system is derived. The original and adjoint systems supply the necessary field information for the rubber cell based sensitivity calculations. Our technique is illustrated through sensitivity analysis of waveguide filters. The estimated sensitivities are used for fast gradient-based optimization and tolerance analysis.

1. INTRODUCTION

Sensitivity analysis plays an important role in the design of microwave circuits. During the optimization procedure, a gradient-based optimizer drives the electromagnetic (EM) simulator. At every iteration, the optimizer requests both the EM response and its gradient with respect to the different design parameters for the current set of parameter values. The response sensitivities are traditionally calculated by perturbing the design parameters one at a time and then using finite difference approximations at the response level. This requires repeated EM simulations of all perturbed EM structures. This process can be time intensive even for a small number of parameters.

The adjoint variable method (AVM) presents a more efficient approach to sensitivity analysis of high frequency structures. AVM

† The first author is now with CIRFE (Center for Integrated RF Engineering), University of Waterloo, Waterloo, ON N2L 3G1, Canada.

was utilized with different numerical EM techniques including the Method of Moments [1], the frequency-domain Transmission Line Modeling (TLM) [2], the Finite Difference Time Domain (FDTD) with unstructured grids [3], and the Beam Propagation Method in photonics [4]. In [5], the AVM technique was used for sensitivity analysis using FDTD with structured grids and for full wave sensitivity analysis of guided wave structures [6]. In [7], it was applied to 2D time-domain TLM problems with structured grids involving non-dispersive boundaries and perfect conducting objects. In all these approaches, using only two full wave EM simulations, the sensitivities of a real objective function, with respect to all design parameters, are estimated regardless of the number of these parameters. This represents significant computational saving as compared to the finite difference approximations.

AVM for time-domain TLM was then developed and extended to handle a variety of practical EM design problems. In [8], and [9], the AVM was adapted to handle problems with dispersive boundaries using the wideband Johns matrix boundaries and the one-way wave-equation absorbing boundaries, respectively. The AVM was also extended to solve a variety of EM structures involving dielectric discontinuities [10], lossy media [11] and full 3D problems [12] using Johns symmetrical condensed node [13]. The approach was further developed for complex responses to calculate network parameters sensitivities e.g. S-parameters [14]. Self-adjoint S-parameters sensitivities were then introduced in [15] for lossless isotropic homogenous media. The self-adjoint technique uses only the original simulation to calculate the sensitivities over a wide frequency band. No adjoint simulations are needed in this case. The original simulations supply both the S-parameters and their sensitivities with respect to all the design parameters over the desired frequency band. In [16], the adjoint-free AVM was applied to lossless isotropic nonhomogenous media as well.

All the above mentioned approaches treat problems with dielectric and metallic discontinuities in a different way. Analytical adjoint systems are derived for the dielectric case, while an approximate adjoint system is utilized for metallic discontinuities. This is mainly because the system matrices are analytical functions of only the material properties. Also, these approaches handle problems with uniform structured grids. Discontinuities are approximated by snapping them to the grid dimensions. However, when optimizing an EM structure, it is important to be able to represent off-grid object boundaries and provide accurate response sensitivities. Different modifications of the symmetric condensed node based TLM were proposed to model non-uniform TLM grids: the hybrid symmetric

condensed node [17] and the multigrid TLM [18]. These techniques accurately model on-grid geometries only. Other efforts to model off-grid objects and boundaries include modifying the scattering matrix of the symmetric condensed node [19], loading it with extra reactive elements [20], and adding extra stubs and/or arms to the boundary TLM nodes [21]. Recently, Huilian et al. introduced in [22] a simple robust approach to model boundaries at arbitrary locations in the TLM symmetric condensed node scheme. This approach depends on modifying the constitutive parameters of the irregular boundary cells. This modification accounts for the irregular boundary positions without changing the cell dimensions. Hence, the computational burden remains low.

In [23], we exploited this recent development. We proposed an AVM approach that exploits the rubber cell concept. Using the modified tensor properties of these cells, we are able to derive an exact adjoint system for both metallic and dielectric discontinuities. Both types of discontinuities are treated in the same way. Utilizing exact adjoint systems improves the accuracy of the algorithm and makes the implementation process easier for any type of discontinuity. In this paper, we further discuss the proposed approach, explaining its implementation and illustrate it with more examples.

We start by giving a brief review of the use of the modified tensor properties to model irregular boundaries in TLM. In Section 3, we develop the necessary modifications in AVM to perform sensitivity analysis of such structures. Section IV discusses the implementational details of the AVM technique exploiting the rubber cell. Section 5 illustrates the efficiency of our algorithm through three examples of different microwave filters. Finally, Section 6 shows how the adjoint sensitivities are used to efficiently optimize a microwave filter and perform tolerance analysis without simulating any perturbed structures.

2. TLM USING RUBBER CELLS

In TLM, both space and time are discretized. The computational domain is modeled through a network of interconnecting transmission lines. The symmetric condensed node is the most common TLM node used for full 3D analysis [13]. Using the symmetric condensed node, all boundaries can only be placed half-way between nodes. Global or local mesh refinements can be used to model arbitrarily shaped boundaries. However, this usually leads to increased computational requirements.

In [22] an efficient method to model boundaries of arbitrary position and shape in TLM was introduced. The method is based on

representing the changes in the dimensions of a TLM cell through an equivalent change of the cell's constitutive parameters. The scattering matrix of a TLM cell of size $\Delta x \times \Delta y \times \Delta z$ and with material properties characterized by the diagonal permittivity and permeability tensors

$$\overleftrightarrow{\varepsilon} = \begin{vmatrix} \varepsilon_{xx} & 0 & 0 \\ 0 & \varepsilon_{yy} & 0 \\ 0 & 0 & \varepsilon_{zz} \end{vmatrix}; \quad \overleftrightarrow{\mu} = \begin{vmatrix} \mu_{xx} & 0 & 0 \\ 0 & \mu_{yy} & 0 \\ 0 & 0 & \mu_{zz} \end{vmatrix} \tag{1}$$

is determined using the general formula given in [22]. For the TLM cell shown in Fig. 1 with scaled dimensions $u\Delta x \times v\Delta y \times w\Delta z$, we modify the tensor permittivities and permeabilities associated with the cell to account for the effect of the size change while preserving its original dimensions.

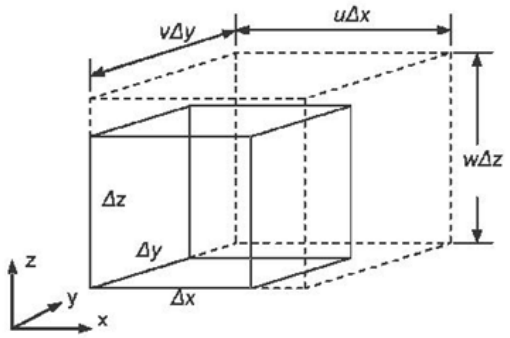

Figure 1. A TLM cell stretched by factors u, v, and w.

The new tensor permittivities and permeabilities are calculated as follows [22]:

$$\begin{aligned} \varepsilon'_{xx} &= \frac{vw}{u}\varepsilon_{xx}, \quad \varepsilon'_{yy} = \frac{uw}{v}\varepsilon_{yy}, \quad \varepsilon'_{zz} = \frac{uv}{w}\varepsilon_{zz} \\ \mu'_{xx} &= \frac{vw}{u}\mu_{xx}, \quad \mu'_{yy} = \frac{uw}{v}\mu_{yy}, \quad \mu'_{zz} = \frac{uv}{w}\mu_{zz} \end{aligned} \tag{2}$$

where u, v, and w are the scaling coefficients in the x, y, and z directions, respectively. After the new tensors are calculated for each deformed cell, the overall scattering matrix is calculated using the general formulae in [22].

Utilizing the rubber cell approach, the TLM simulation carries out a sequence of scattering and connection steps. The complete TLM step for nondispersive boundaries is given by

$$V_{k+1} = CSV_k + V_k^s \tag{3}$$

where V_k is the vector of incident impulses for all nodes at the kth time step. S and C are the global scattering and connection matrices, respectively. The vector V_k^s is the vector of source excitation at the kth time step.

3. AVM THEORY

Following the discussion in Section 2, we conclude that any off-grid discontinuity, whether it is a perfectly conductive obstacle or a dielectric insert, can be modeled by an on-grid discontinuity surrounded by rubber cells with modified tensors. Accordingly, a slight perturbation of a discontinuity results in a perturbation in the surrounding cells tensors. This directly leads to an explicit perturbation in the nodal scattering matrix of those cells. Hence, the perturbation can be modeled as an analytical perturbation in the overall scattering matrix in a way similar to the case of perturbing a dielectric discontinuity [10].

To calculate the sensitivity of a real objective function F with respect to a design parameter x_i, we follow the derivation presented in [10]. We make use of the analytical derivative of the system matrix A with respect to the tensor properties of the perturbed TLM cells surrounding the discontinuity. The sensitivity is calculating using the sensitivity expression [10]

$$\frac{\partial F}{\partial x_i} \approx \frac{\partial^e F}{\partial x_i} - \Delta t \sum_{k=0}^{N_t} \lambda_k^T \frac{\partial A}{\partial x_i} V_k, \quad i = 1, 2, \ldots, n \tag{4}$$

where N_t is the total number of simulation time steps and λ_k is the vector of adjoint impulses. λ_k is calculated using the exact adjoint system [10]:

$$\lambda_{k-1} = S^T C^T \lambda_k - V_k^{s,\lambda} \tag{5}$$

where $V_k^{s,\lambda}$ is the vector of adjoint excitation calculated during the original simulation.

To calculate the derivative of the system matrix with respect to the design parameter of interest, we consider a case of a general 3D perturbation. For such a perturbation, it is possible that a cell is perturbed in any of the three directions. Using the chain rule:

$$\frac{\partial A}{\partial x_i} = \frac{\partial A}{\partial u} \cdot \frac{\Delta u}{\Delta x_i} + \frac{\partial A}{\partial v} \cdot \frac{\Delta v}{\Delta x_i} + \frac{\partial A}{\partial w} \cdot \frac{\Delta w}{\Delta x_i}. \tag{6}$$

Then using the chain rule again we have:

$$\begin{aligned}
\frac{\partial A}{\partial u} =& \frac{\partial A}{\partial \varepsilon'_{xx}} \cdot \frac{\partial \varepsilon'_{xx}}{\partial u} + \frac{\partial A}{\partial \varepsilon'_{yy}} \cdot \frac{\partial \varepsilon'_{yy}}{\partial u} + \frac{\partial A}{\partial \varepsilon'_{zz}} \cdot \frac{\partial \varepsilon'_{zz}}{\partial u} \\
&+ \frac{\partial A}{\partial \mu'_{xx}} \cdot \frac{\partial \mu'_{xx}}{\partial u} + \frac{\partial A}{\partial \mu'_{yy}} \cdot \frac{\partial \mu'_{yy}}{\partial u} + \frac{\partial A}{\partial \mu'_{zz}} \cdot \frac{\partial \mu'_{zz}}{\partial u} \\
\frac{\partial A}{\partial v} =& \frac{\partial A}{\partial \varepsilon'_{xx}} \cdot \frac{\partial \varepsilon'_{xx}}{\partial v} + \frac{\partial A}{\partial \varepsilon'_{yy}} \cdot \frac{\partial \varepsilon'_{yy}}{\partial v} + \frac{\partial A}{\partial \varepsilon'_{zz}} \cdot \frac{\partial \varepsilon'_{zz}}{\partial v} \\
&+ \frac{\partial A}{\partial \mu'_{xx}} \cdot \frac{\partial \mu'_{xx}}{\partial v} + \frac{\partial A}{\partial \mu'_{yy}} \cdot \frac{\partial \mu'_{yy}}{\partial v} + \frac{\partial A}{\partial \mu'_{zz}} \cdot \frac{\partial \mu'_{zz}}{\partial v} \\
\frac{\partial A}{\partial w} =& \frac{\partial A}{\partial \varepsilon'_{xx}} \cdot \frac{\partial \varepsilon'_{xx}}{\partial w} + \frac{\partial A}{\partial \varepsilon'_{yy}} \cdot \frac{\partial \varepsilon'_{yy}}{\partial w} + \frac{\partial A}{\partial \varepsilon'_{zz}} \cdot \frac{\partial \varepsilon'_{zz}}{\partial w} \\
&+ \frac{\partial A}{\partial \mu'_{xx}} \cdot \frac{\partial \mu'_{xx}}{\partial w} + \frac{\partial A}{\partial \mu'_{yy}} \cdot \frac{\partial \mu'_{yy}}{\partial w} + \frac{\partial A}{\partial \mu'_{zz}} \cdot \frac{\partial \mu'_{zz}}{\partial w}
\end{aligned} \tag{7}$$

Since the matrix A is an analytical function of the tensors, its derivatives with respect to the tensors can be analytically calculated. Using (2), (6), and (7), the analytic derivatives of A with respect to x_i, $i = 1, 2, \ldots, n$, are calculated. They are then used in the sensitivity expressions (4).

There are many advantages of this technique. First is the ability to model any discontinuity without the need to snap it to the grid. Second, the use of analytical derivatives of the system matrices to model the perturbations increases the algorithm accuracy and simplifies the implementation.

Finally no mapping approximation [8] is needed and an exact adjoint system is used for both metallic and dielectric discontinuities.

4. IMPLEMENTATION DETAILS

In [12], the implementation process of the AVM technique in 3D problems using the symmetric condensed node was explained. Figs. 2 and 3 show the nodes affected and the links to be stored when perturbing a perfectly conducting and a dielectric discontinuity, respectively.

Using Johns symmetric condensed node, a perturbation in a metallic discontinuity changes the way impulses are connected around it. This affects only the global connection matrix. On the other hand, when a dielectric discontinuity is perturbed, the perturbation causes a local change of the dielectric constant. This translates into

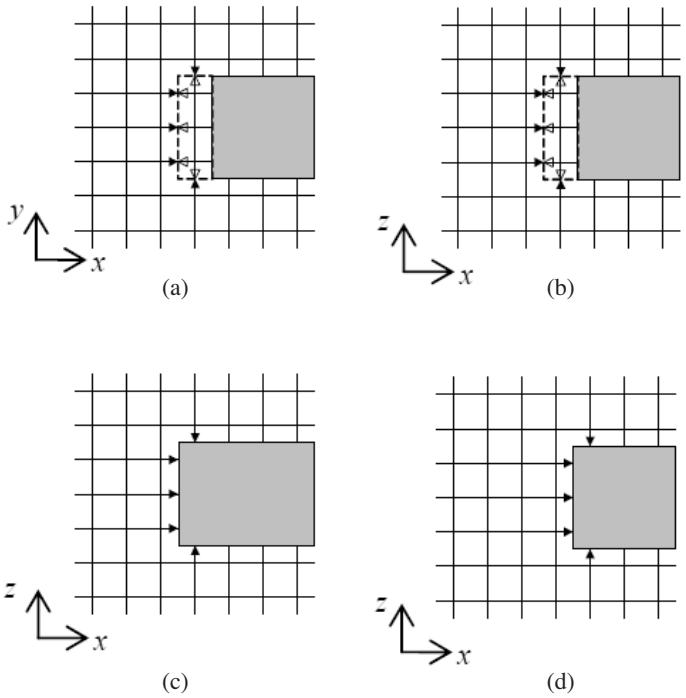

Figure 2. A perturbation of a perfectly conducting discontinuity: (a) impulses stored in original system (top view), (b) impulses stored in original system (side view), (c) impulses stored in exact perturbed adjoint system, and (d) impulses stored in approximate unperturbed adjoint system [12].

a perturbation of the scattering matrix of the surrounding nodes. In the rubber cell, the perturbation of a design parameter of either a metallic or a dielectric discontinuity perturbs the nodal scattering matrix of the nodes affected by this particular design parameter. The implementation details are explained in more detail in this section for both types of discontinuities.

4.1. Metallic Discontinuities

To illustrate the actual implementation of AVM for rubber cells, consider the off-grid metallic discontinuity shown in Fig. 4(a). For simplicity, we illustrate a 2D case. Using the rubber cells, the discontinuity is snapped to the symmetric condensed node grid and then it is surrounded by cells with modified tensor properties as shown

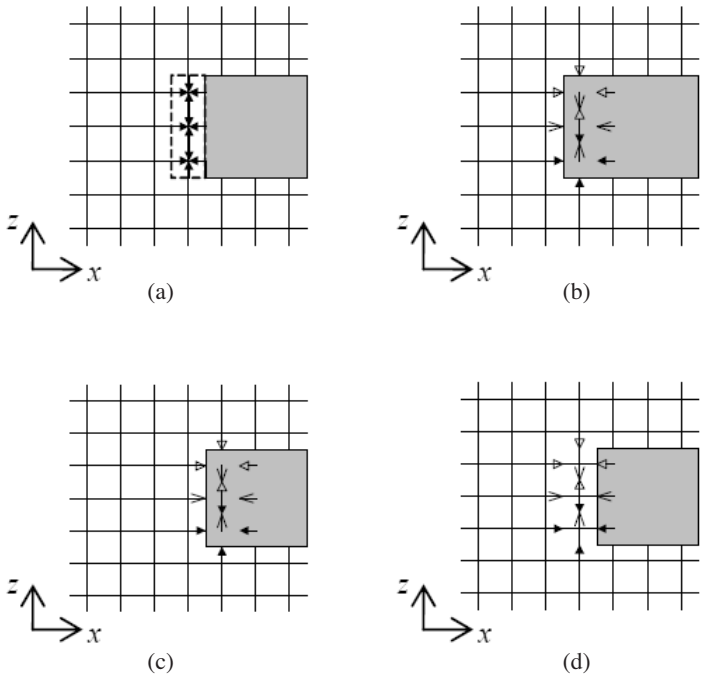

Figure 3. A perturbation of a dielectric discontinuity: (a) impulses stored in original system, (b) impulses stored in exact perturbed adjoint system, (c) impulses stored in approximate unperturbed adjoint system, and (d) impulses stored in exact unperturbed adjoint system [12] (each group of similar arrows represent impulses to be stored for a particular node).

in Fig. 4(b). The stretching and shrinkage factors of the rubber cells are also shown. The sensitivity expression (4) requires storing voltage impulses in both the original and adjoint simulations. In the original simulation, we store the impulses reflected from the nodes whose scattering matrices are affected by the perturbation of the particular discontinuity.

In the adjoint simulation, we store the reflected impulses on the links connected to those links used in the original simulation. Figs. 4(c) and 4(d) show the cells affected by a perturbation in the positive x- and z-directions, respectively. We store the incident voltages on those cells in the original simulation and their respective reflected impulses in the adjoint simulation.

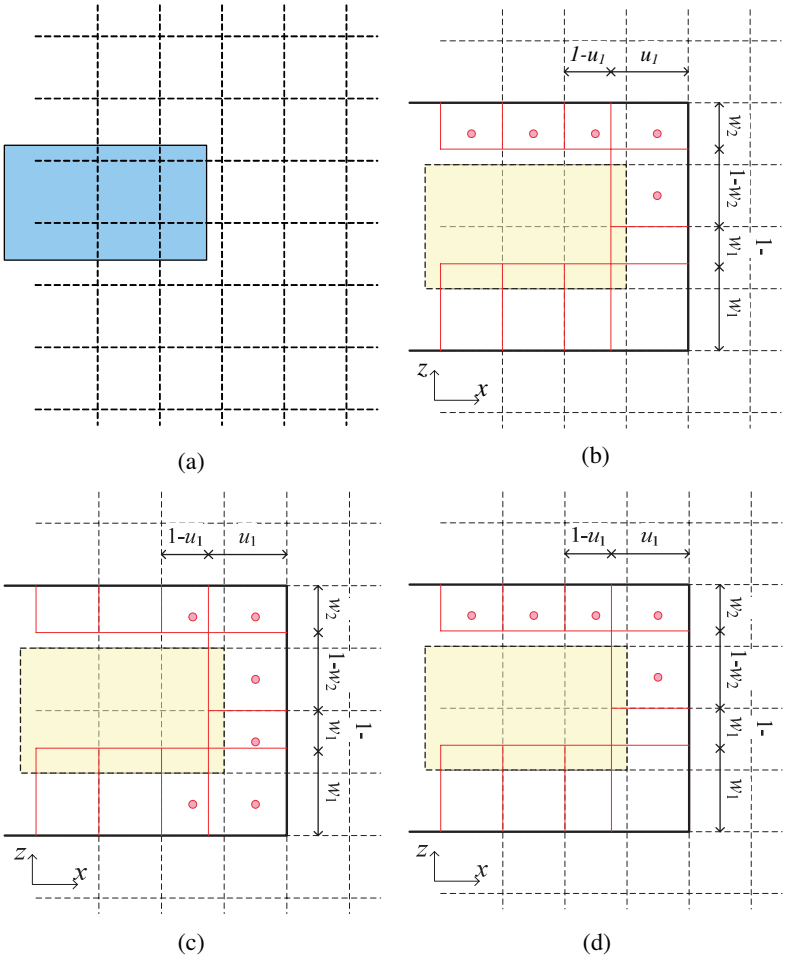

Figure 4. Rubber cell implementation for a metallic discontinuity; (a) the off-grid discontinuity, (b) the snapped to grid discontinuity showing the sizing factors of the rubber cells, (c) the nodes to be stored due to a perturbation in the positive x direction, and (d) the nodes to be stored due to a perturbation in the positive z direction.

4.2. Dielectric Discontinuities

An off-grid dielectric discontinuity can be also modeled using the rubber cell. The geometry is approximated by a snapped-to-the-grid object surrounded by rubber cells to account for the scaling of the nodes. In addition, the boundary nodes of the dielectric discontinuity

need to be replaced by rubber cells as well. This is the main difference between this case and that of metallic discontinuities. Fig. 5(a) shows an off-grid 2D dielectric object and Fig. 5(b) shows how it is modeled using rubber cells. Rubber cells are marked with dots in their centers.

When the dielectric object is perturbed in a certain direction, the scaling factors of both the external and internal boundary nodes are

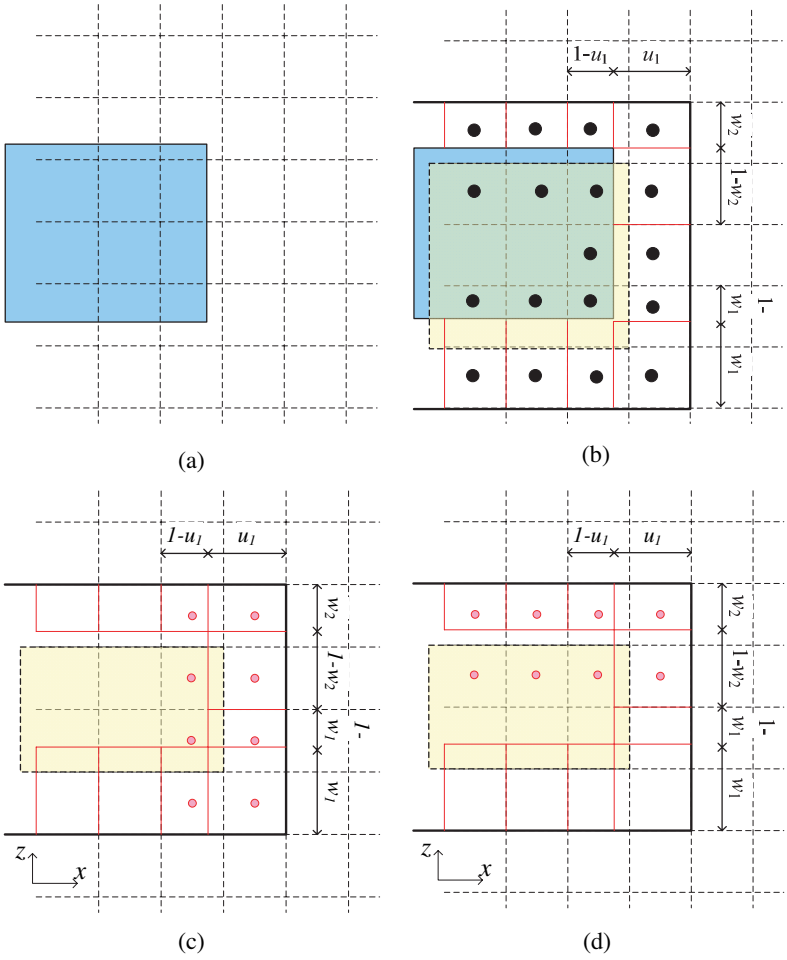

Figure 5. Rubber cell implementation for a dielectric discontinuity; (a) the offgrid discontinuity, (b) the snapped to grid discontinuity showing the sizing factors of the rubber cells, (c) the nodes to be stored due to a perturbation in the positive x direction, and (d) the nodes to be stored due to a perturbation in the positive z direction.

changed. Accordingly, we need to store impulses reflected for these two types of nodes. Figs. 5(c) and 5(d) show the nodes affected by perturbation in the positive x- and z-directions, respectively. Accordingly, we store the incident voltages on those cells in the original simulation and their respective reflected impulses in the adjoint simulation.

5. EXAMPLES

The examples presented in this section are simulated using our in-house TLM simulator coded in Matlab [24]. AVM sensitivities are compared to central finite difference sensitivities calculated at the response level. The response of interest is the absolute value of the S-parameters. Our algorithm provides sensitivities of the real and imaginary parts of the S-parameters. Accordingly, we can also calculate the sensitivities of the magnitude and phase of the S-parameters. The sensitivities of the magnitude are obtained using the formula:

$$\frac{\partial |S_{pq}|}{\partial x_i} = \frac{\mathrm{Re}\{S_{pq}\}\left(\frac{\partial \mathrm{Re}\{S_{pq}\}}{\partial x_i}\right) + \mathrm{Im}\{S_{pq}\}\left(\frac{\partial \mathrm{Im}\{S_{pq}\}}{\partial x_i}\right)}{|S_{pq}|} \tag{8}$$

where p and q represent the ports number; p, $q = 1, 2, \ldots, N$.

5.1. Three-Resonator Waveguide Filter [15]

The filter is shown in Fig. 6. The waveguide width is $a = 60.0\,\mathrm{mm}$ and its length is $180.0\,\mathrm{mm}$. The cell size is $\Delta l = 1.5\,\mathrm{mm}$. Johns matrix boundaries are used to model the dispersive waveguide ports. Symmetry is used to simulate only half of the structure.

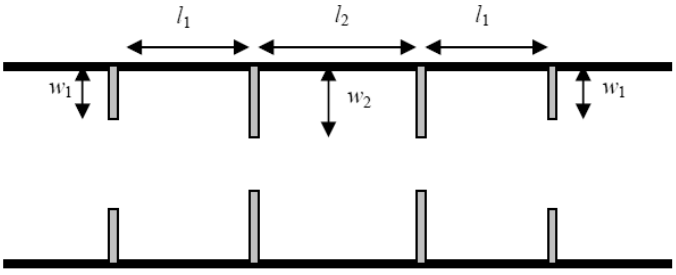

Figure 6. A three-resonator waveguide filter.

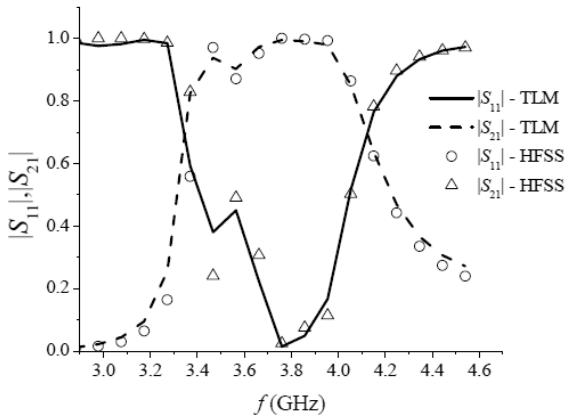

Figure 7. Return and insertion losses for the three-resonator waveguide filter.

The design parameters are the iris widths w_1 and w_2, and the resonator lengths l_1 and l_2. The nominal values are $[w_1\ w_2\ l_1\ l_2]^T = [14.0\ 17.0\ 40.0\ 45.0]^T$ mm and the irises have zero thickness. Fig. 7 shows the S-parameters calculated using our in-house TLM simulator employing the rubber cell implementation in comparison with the S-parameters calculated using HFSS [25].Very good agreement is obtained between the two simulators. Fig. 8 shows the S-parameters sensitivities calculated with respect to all the design parameters. Good agreement is obtained at most frequencies except at frequencies where the response is highly nonlinear. Using central-difference calculations at the response level requires 8 additional simulations. Using AVM only 2 full simulations are required. AVM simulations required 473 seconds for the original system, 491 seconds for the adjoint system, and 289 seconds for the postprocessing calculations of the sensitivities. The total is 1253 for 4 parameters and 29 frequencies. On the other hand using HFSS and central differences required a total of $9 \times 172 = 1548$ seconds for .1in TLM lies in the use of the rubber cell that requires using a smaller time step to ensure stability.

5.2. Dielectric Resonator Filter [11]

The S-parameter sensitivities of the dielectric resonator filter shown in Fig. 9 are also calculated using our AVM approach. The width of the waveguide is 60.0 mm, with $\Delta l = 1.5$ mm. The waveguide length is 150.0 mm. The sensitivities are calculated with respect to the width w and the thickness d of the dielectric posts. The

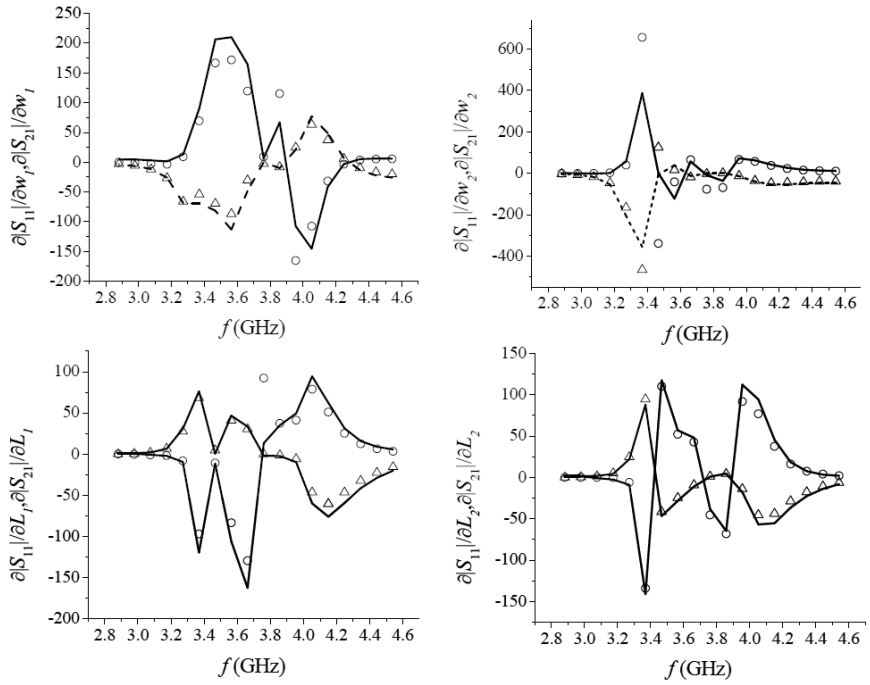

Figure 8. Return loss and insertion loss sensitivities for the three-resonator waveguide filter; $|S_{11}|$ sensitivities calculated using central-differences (—); $|S_{11}|$ sensitivities calculated using AVM (○); $|S_{21}|$ sensitivities calculated using central-differences (- -); and $|S_{21}|$ sensitivities calculated using AVM (△).

dielectric permittivity is $\varepsilon_r = 4.0$. The S-parameter sensitivities are estimated over a range of frequencies where only the dominant mode is propagating. The sensitivities are calculated at $[w\ d\ s]^T = [18.86\ 11.32\ 37.0]^T$ mm and compared to central-difference sensitivities in Fig. 10. Central-difference calculations require 6 extra simulations, while AVM calculations require only one extra TLM simulation.

5.3. An Evanescent Mode Waveguide Filter [26]

The evanescent mode filter is shown in Fig. 11(a). It consists of alternating dielectric and air sections. The input and output sections of the filter are dielectric-filled. The main advantage of this filter is achieving a smaller structure, besides decreasing manufacturing

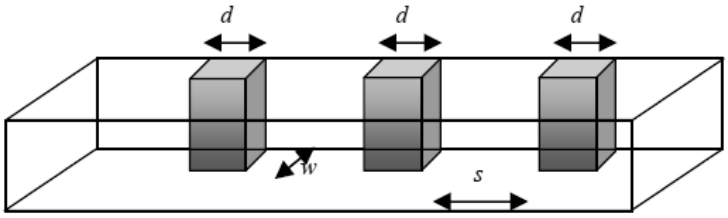

Figure 9. The dielectric resonator filter.

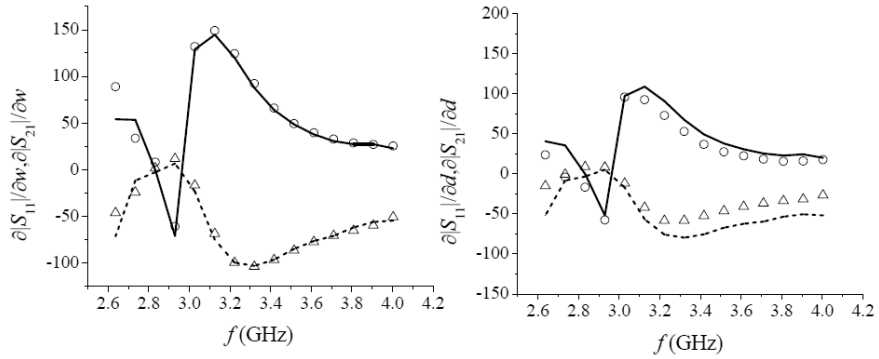

Figure 10. Return loss and insertion loss sensitivities for the dielectric resonator filter; $|S_{11}|$ sensitivities calculated using central-differences (—); $|S_{11}|$ sensitivities calculated using AVM (○); $|S_{21}|$ sensitivities calculated using central-differences (- -); and $|S_{21}|$ sensitivities calculated using AVM (△).

tolerances compared to metallic iris waveguides.

The waveguide width is 40.0 mm. The dielectric used has $\varepsilon_r = 2.54$. The cell size is 1.0 mm. The structure is symmetrical with respect to its 2 ports. The lengths of the air sections are $l_1 = 13.0$ mm and $l_2 = 23.0$ mm. The two dielectric sections are of equal lengths $l_3 = 23.0$ mm. The filter is designed and optimized using the mode matching solver μWave Wizard [27]. A comparison between the filter responses obtained using mode matching and using our in-house TLM simulator is shown in Fig. 11(b). Fig. 12 compares the return and insertion loss sensitivities calculated using AVM and using central differences. Good agreement is obtained for the two approaches except at some frequencies due to the high nonlinearity of the filter frequency response. The results also agree with the published results in [16] for the same example without using the rubber cell.

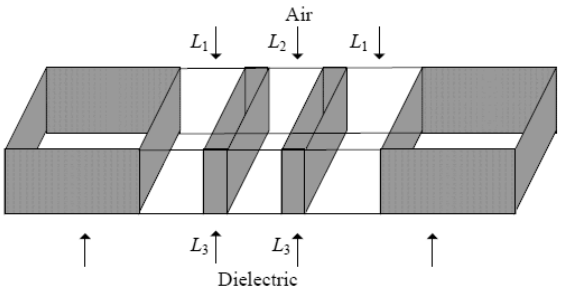

(a)

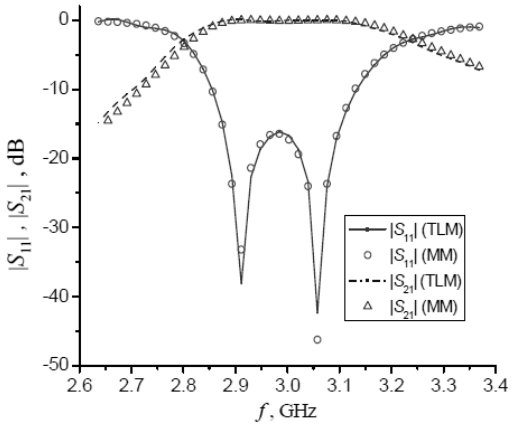

(b)

Figure 11. Evanescent mode waveguide filter: (a) 3-D layout and, (b) the reflection and insertion loss (MM: mode matching).

6. APPLICATIONS OF AVM

In the previous sections we showed how the AVM offers an efficient approach for sensitivity analysis in EM numerical simulations. In this section we present how the AVM sensitivities can be directly used to significantly improve the efficiency of EM design optimization and tolerance analysis.

6.1. Gradient Based Optimization

In this example we use the AVM sensitivities to optimize the three resonator filter presented in Section 5. The design parameters are the iris widths and the resonator lengths. In total we have four

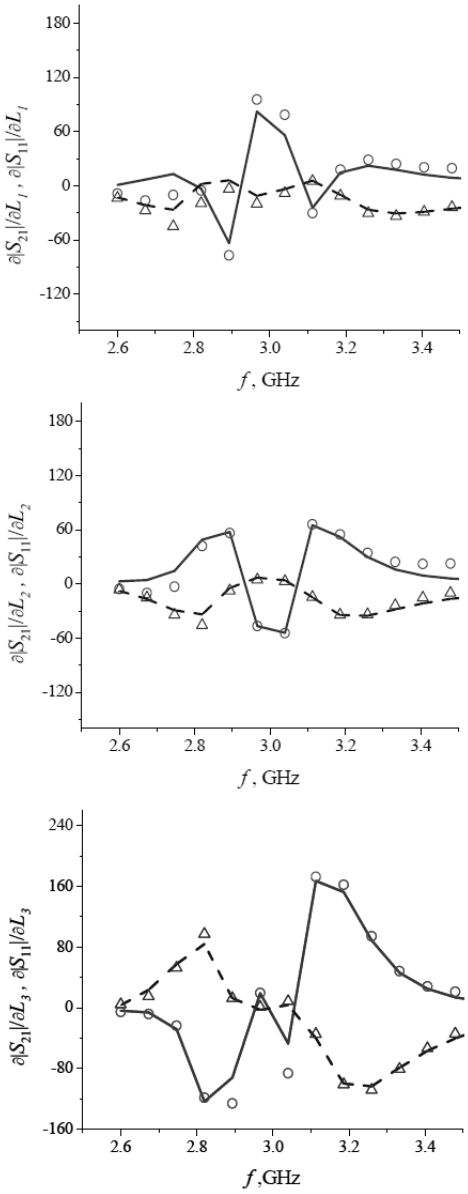

Figure 12. Return loss and insertion loss sensitivities for the evanescent mode filter; $|S_{11}|$ sensitivities calculated using central-differences (—); $|S_{11}|$ sensitivities calculated using AVM (○); $|S_{21}|$ sensitivities calculated using central-differences (- -); and $|S_{21}|$ sensitivities calculated using AVM (△).

optimization variables. The design specifications for this filter are:

$$\begin{array}{lll} |S_{11}| \geq 0.9 & \text{for} & 2.8\,\text{GHz} \leq f \leq 3.27\,\text{GHz} \\ |S_{11}| \leq 0.15 & \text{for} & 3.46\,\text{GHz} \leq f \leq 3.95\,\text{GHz}. \\ |S_{11}| \geq 0.9 & \text{for} & 4.34\,\text{GHz} \leq f \leq 5.34\,\text{GHz} \end{array} \tag{9}$$

The initial values of the design parameters are $[w_1\ w_2\ l_1\ l_2]^T = [14.0\ 17.0\ 40.0\ 45.0]^T$ mm. The filter response for these values is shown in Fig. 13 together with the design requirements. Optimization is done using the Matlab [23] minimax optimization algorithm. Gradients calculated using the AVM are provided at every optimization iteration. The optimizer reached the optimal set of parameters after 6 iterations using only 14 function evaluations including those needed for the line search performed per iteration. This means 6 AVM simulations in addition to 8 function evaluations for line search. This is equivalent to a total of 20 TLM simulations. If finite-difference approximations were used, we would need 5 functions evaluations per iteration in addition to the 8 function evaluations for line search resulting in a total of 38 EM simulations.

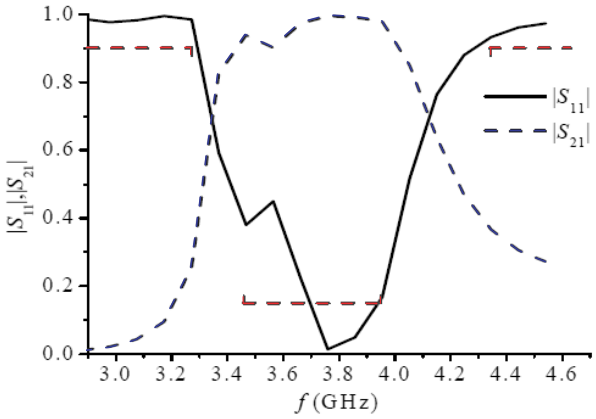

Figure 13. S-parameters for the three-resonator filter showing the required design specifications.

It is clear that AVM achieves almost 50% computational savings in the whole optimization process. These savings will be more significant for a problem with larger number of design variables. The optimal values for the design parameters are $[w_1\ w_2\ l_1\ l_2]^T = [13.0998\ 17.1969\ 40.2254\ 43.4182]^T$ mm. The optimized filter response is shown in Fig. 14.

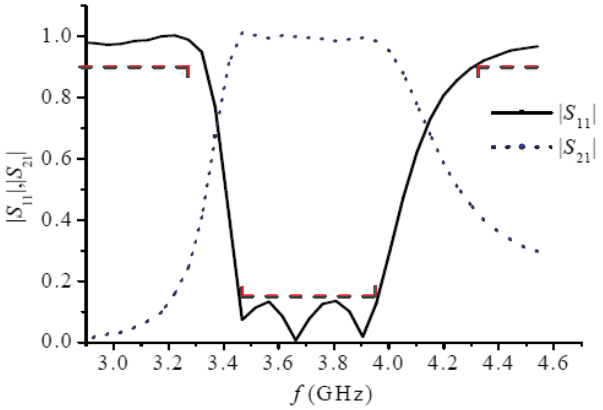

Figure 14. The optimized filter response.

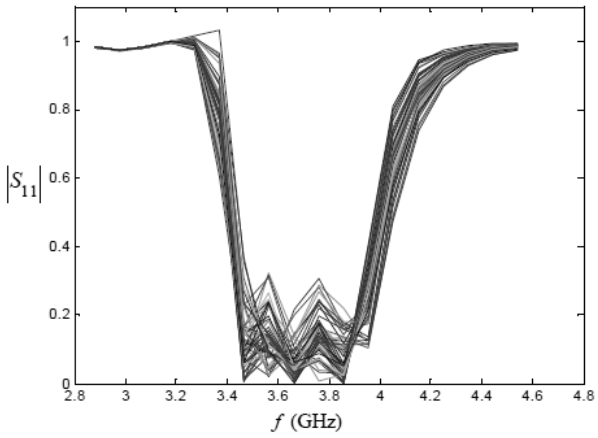

Figure 15. The tolerance analysis curves for the three-resonators filter.

6.2. Tolerance Analysis

Tolerance and yield analysis use the EM simulator to determine a priori the percentage of defective products produced by the fabrication process due to manufacturing tolerances. Tolerance analysis involves performing hundreds of full-wave simulations employing small perturbations in the optimized design.

Since AVM provides response gradients in an efficient way, we used them to predict the response of the optimal design with small tolerances. Using Taylor's expansion, the response of the slightly perturbed design can be predicted to be

$$|S_{11}(x+\Delta x)| = |S_{11}(x)| + \left[\frac{\partial |S_{11}|}{\partial x}\right]^T \cdot \Delta x \tag{10}$$

where Δx lies within the manufacturing tolerance of the process used. Equation (10) is calculated hundreds of times using randomly chosen values for Δx to predict the response of the optimal design when affected by the tolerances. This means only one full wave AVM simulation is needed to perform a complete tolerance analysis. Fig. 15 shows tolerance analysis for the optimized three-resonator waveguide filter example. The tolerance used is 10%.

7. CONCLUSION

The AVM is applied for the first time to TLM problems with conformal boundary modeling. This conformal modeling is achieved using TLM rubber cells with modified tensors to model irregular cells. Using this novel technique, all perturbations can be modeled as analytical perturbations of the global scattering matrix. The availability of the analytical derivative of the system matrix with respect to any design parameter enables us to derive an exact adjoint system, thus increasing the algorithm accuracy, while simplifying its implementation. We utilized the AVM sensitivities to illustrate efficient gradient-based optimization and tolerance analysis.

REFERENCES

1. Georgieva, N. K., S. Glavic, M. H. Bakr, and J. W. Bandler, "Feasible adjoint sensitivity technique for EM design optimization," *IEEE MTT-S Int. Microwave Symp. Dig.*, Vol. 1, 299–302, Jun. 2003.
2. Bakr, M. H. and N. K. Georgieva, "An adjoint variable method for frequency domain TLM problems with conducting boundaries," *IEEE Microwave & Wireless Comp. Letters*, Vol. 13, 408–410, Nov. 2003.
3. Chung, Y. S., C. Cheon, I. H. Park, and S. Y. Hahn, "Optimal design methods for microwave devices using time domain method and design sensitivity analysis-part II: FDTD case," *IEEE Trans. Microwave Theory and Tech.*, Vol. 37, 3255–3295, Sep. 2001.

4. Swillam, M. A., M. H. Bakr, and X. Li, "Efficient adjoint sensitivity analysis exploiting the FD-BPM," *J. Lightwave Technology*, Vol. 25, 1861–1869, Jul. 2007.
5. Shen, G., H. W. W. Tam, N. K. Nikolova, and M. H. Bakr, "Adjoint sensitivity technique for FDTD methods on structured grids," *IEEE Int. Symp. Antennas & Propagation*, 746–749, Columbus, OH, 2003.
6. Swillam, M. A., M. H. Bakr, and X. Li, "Full wave sebsitivity analysis of guided wave structures using FDTD," *J. Electromagnetics Waves and Applications*, Vol. 22, No. 16, 2135–2145, 2008.
7. Bakr, M. H. and N. K. Nikolova, "An adjoint variable method for time-domain transmission-line modeling with fixed structured grids," *IEEE Trans. Microwave Theory and Tech.*, Vol. 52, 554–559, Feb. 2004.
8. Bakr, M. H. and N. K. Nikolova, "An adjoint variable method for time domain TLM with wideband Johns matrix boundaries," *IEEE Trans. Microwave Theory and Tech.*, Vol. 52, 678–685, Feb. 2004.
9. Basl, P. A. W., M. H. Bakr, and N. K. Nikolova, "Time-domain sensitivity analysis of planar structures using first-order one-way wave equation boundaries," *Int. Journal. of Numerical Modelling: Electronic Networks, Devices and Fields*, to be published.
10. Basl, P. A. W., M. H. Bakr, and N. K. Nikolova, "Efficient estimation of sensitivities in TLM with dielectric discontinuities," *IEEE Microwave & Wireless Comp. Letters*, Vol. 15, 89–91, Feb. 2005.
11. Basl, P. A. W., M. H. Bakr, and N. K. Nikolova, "Efficient sensitivity analysis of lossy discontinuities using time-domain TLM," *Antem/URSI 2006 Conference Proc.*, 613–616, Jul. 2006.
12. Basl, P. A. W., M. H. Bakr, and N. K. Nikolova, "An AVM technique for 3-D TLM with symmetric condensed nodes," *IEEE Microwave & Wireless Comp. Letters*, Vol. 15, 618–620, Oct. 2005.
13. Johns, P. B., "Symmetrical condensed node for the TLM method," *IEEE Trans. Microwave Theory and Tech.*, Vol. 35, 370–377, Feb. 1987.
14. Bakr, M. H. and N. K. Nikolova, "Efficient estimation of adjointvariable S-parameter sensitivities with time domain TLM," *Int. Journal of Numerical Modelling: Electronic Networks, Devices and Fields*, Vol. 18, No. 2, 171–187, Mar. 2005.
15. Bakr, M. H., N. K. Nikolova, and P. A. W. Basl, "Self-

adjoint S-parameter sensitivities for lossless homogeneous TLM problems," *Int. Journal of Numerical Modelling: Electronic Networks, Devices and Fields*, Vol. 18, 441–455, Nov. 2005.

16. Basl, P. A. W., M. H. Bakr, and N. K. Nikolova, "Theory of selfadjoint S-parameter sensitivities for lossless nonhomogeneous transmission-line modeling problems," *IET Proc. Microwaves, Antennas & Propagation*, to be published.
17. Scaramuzza, R. A. and A. J. Lowery, "Hybrid symmetrical condensed node for the TLM method," *Electronics Letters*, Vol. 26, 1947–1949, Nov. 1990.
18. Herring, J. L. and C. Christopoulos, "Multigrid transmission-line modeling method for solving electromagnetic field problems," *Electronics Letters*, Vol. 27, 1794–1795, Sep. 1991.
19. German, F. G., "Infinitesimally adjustable boundaries in symmetrical condensed node TLM simulation," *Applied Electromagnetics Symp. Dig.*, 482–490, Monterey, CA, 1993.
20. Muller, U., A. Beyer, and W. J. R. Hoefer, "Moving boundaries in 2-D and 3-D TLM simulations realized by recursive formulas," *IEEE Trans. Microwave Thoery and Tech.*, Vol. 40, 2267–2271, Dec. 1992.
21. Gwarek, W. K., "Analysis of an arbitrarily-shaped planar circuit a time-domain approach," *IEEE Trans. Microwave Thoery and Tech.*, Vol. 33, 1067–1072, Oct. 1985.
22. Huilian, D., S. Poman, and W. J. R. Hoefer, "Cells with tensor properties for conformal TLM boundary modeling," *2006 IEEE MTT-S Int. Microwave Symp.*, Vol. 11, 157–160, San Francisco, CA, USA, 2006.
23. Basl, P. A. W., M. H. Bakr, and N. K. Nikolova, "Efficient transmission line modeling sensitivity analysis exploiting rubber cells," *IEEE MTT-S Conference Proc.*, 53–56, June 2008.
24. Mathworks, Matlab, "R2007," ed., 2007. www.mathworks.com
25. Ansoft Corporation, "HFSS," 9.2.1 ed., 2004. www.ansoft.com
26. Beneat, J., "Design of high frequency filters for data transmission & evanescent mode waveguide structures," PhD thesis, Univ. de Bordeux, 1993.
27. μWave Wizard ver. 5.6,2006, Mician, Bremen, Germany. www.mician.com